*Acta Polytechnica CTU Proceedings* **44**:19–27, 2023
https://doi.org/10.14311/APP.2023.44.0019

Published by the Czech Technical University in Prague

# NEUTRONIC ANALYSIS OF A HEAT-PIPE COOLED REACTOR

Josef Sabol*, Jan Frýbort

*Czech Technical University in Prague, Faculty of Nuclear Sciences and Physical Engineering, Department of Nuclear Reactors, V Holešovičkách 2, 180 00 Prague 8, Czech Republic*

* corresponding author: saboljos@cvut.cz

Abstract. Heat-pipe cooled reactors belong to the group of nuclear reactors using heat pipes filled with liquid metals (such as sodium or potassium) to cool the core. Due to the passive heat removal system, there is no need to use closed loops with pumps, and the reactor can be operated with reduced operational requirements. Consequently, this system can be used in remote locations without access to an electrical grid, or it can be used for space applications.

This paper deals with a neutronic study of the Special Purpose Reactor Design-B concept from the Idaho National Laboratory. Using Monte Carlo code Serpent 2 and ENDF/B VIII.0 library, a fixed-temperature model was created to calculate the safety characteristics of the system. This included reactivity coefficients, power distribution, neutron flux spectrum, and criticality safety. In a simplified depletion calculation, an effect of fuel depletion on safety systems was determined as well as a decay heat.

Keywords: Heat pipe, nuclear reactor, space, neutronic analysis, Serpent 2.

## 1. Introduction

Heat-pipe cooled (HPC) reactors belong to the group of nuclear reactors using heat pipes filled with liquid metals (such as sodium or potassium) to cool the core. They are composed of a reactor core, heat pipes, reflector, regulation system, shielding, and electrical conversion system. Due to the passive heat removal system, there is no need to use closed cooling loops with pumps inside the reactor core, and the reactor can be operated with reduced requirements for external systems. Consequently, this system can be used in remote locations without access to an electrical grid (such as research and military stations), or it can be used for space applications (Moon bases or spacecrafts).

Heat pipes are devices operating on the principle of natural convection and phase change, being capable of heat transfer with a tiny temperature gradient. They consist of a tube and working fluid. At the level of reactor core, the working fluid is operating at its boiling point, gradually receiving latent heat and then evaporates, resulting in local pressure increase. Due to the pressure drop, the vaporized substance moves to the other end of the tube, where it releases latent heat, condenses, and flows back along the reactor walls to the core. To function properly, a porous cover is used to cover the inner wall of the tubes. This cover keeps the liquid on the walls through the capillary effect. Because of the above mentioned, it is possible to use the tubes in any orientation, against gravity and even in space applications [1].

The idea of HPC reactors originated in the 1990s at Los Alamos National Laboratory (LANL), as a power source for space applications. It was supposed to be a group of small modular units with a variable electric power output of up to 100 kW, with an operation period of at least 10 years and with a focus on safe and trouble-free operation [2]. The first designs of HPC reactors from LANL were SAFE (designed for use in satellites and spacecrafts) [3] and HOMER (designed for planetary applications) [4] reactor concepts. However, neither of these projects was ever implemented. There was only a test of sodium heat pipes, a Stirling engine, and an ion thruster as part of the non-nuclear SAFE-30 experiment between the years 2000 and 2001 [5].

After a long lack of interest in space exploration, a new initiative to revive the HPC reactor project came in the 2010s. LANL started the development of Kilopower reactors specifically designed for space applications. These reactors were designed to generate electric power output up to 10 kW and were based on the use of sodium heat pipes, high-enriched uranium, BeO reflector, and Stirling engines for energy conversion. This project ended with a successful test of KRUSTY reactor in 2018 [6].

At the same time as the Kilopwer project, another concept called Megapower reactors was under development, operating on a similar principle. These reactors are based on the usage of a low-enriched uranium (up to 20 % in form of $UO_2$ or UN), potassium or sodium heat pipes, $Al_2O_3$ reflector with $B_4C$ control drums used to control the reactivity, heat transfer medium from stainless steel or molybdenum and an energy conversion system based on an open Brayton cycle. Due to the greater heat power output (up to 5 or 15 MW), the reactor would possibly operate exclusively in terrestrial applications, such as research or military stations [7].

In 2017, a study was proposed at Idaho National

Laboratory (INL) that tried to identify potential safety and technical problems associated with the Megapower reactor. Some of the frequently mentioned problems are, for example, fabrication of compact stainless steel serving as a heat transfer medium, and stress strain and volumetric expansion of stainless steel when one of the heat pipes fails [8]. In addition to small modifications of the design to make the reactor possible to manufacture, two alternative designs were established that completely avoid the mentioned problems. Referred to as a Special Purpose Reactor (SPR) Design-A and Design-B, these designs work on the same principle and differ only in the reactor core design [1].

This technology provide a suitable alternative for passive heat removal systems in space nuclear reactors, or they can also be used in terrestrial conditions. To use them in the future, it is necessary to understand more about the neutronic and thermohydraulic properties of these devices. However, since heat pipes are still a new technology with a lack of experimental data, it has to rely on numerical simulations for now, which could serve as a basis for experimental testing in the future.

This paper further deals with a detailed neutronic study of the SPR Design-B reactor concept from INL, and it focuses mainly on safety analysis during depletion.

## 2. Neutronic Model

### 2.1. Software

The neutron transport and the depletion calculations were performed using stochastic Monte-Carlo code Serpent 2 in version 2.1.32 [9] and with nuclear data library ENDF/B-VIII.0 [10].

In the calculations with multiplication factor $k_{\text{eff}}$, 1 000 000 neutrons were used to simulate the particle transport, 100 inactive cycles to stabilize the neutron distribution and 1 500 active cycles to collect the results. For the depletion calculations, 100 000 simulated neutrons were used in 1 000 active and 100 inactive cycles.

### 2.2. Reactor Design

The thermal power of the SPR Design-B reactor is 5 MW. All dimensions, materials, and temperatures are taken from [1]. Parameters of individual components are presented in Table 6 in Appendix A. The thermodynamic properties of potassium were taken from [11], sodium from [12], and helium from [13]. The composition of 316 stainless steel (SS316) is taken from [14]. The isotopic composition of the elements is natural according to [15]. The horizontal and vertical cross sections of the model are shown in Figure 10 in Appendix A.

For safety reasons, the reactor core is divided into 6 segments separated by double SS316 wall, each segment contains 352 fuel rods and 204 heat pipes.

| | $\rho_0$ [g/cm$^3$] | $\bar{\alpha}$ [1/K] |
|---|---|---|
| $UO_2$ | 10.52 [1] | $10.08 \cdot 10^{-6}$ [16] |
| SS316 | 8.00 [14] | $19.30 \cdot 10^{-6}$ [17] |
| $Al_2O_3$ | 3.95 [18] | $8.50 \cdot 10^{-6}$ [18] |
| $B_4C$ | 2.51 [1] | - |

Table 1. Densities and thermal expansion coefficients for used materials.

The fuel rod is 150 cm long, followed by a 2 cm gas plenum. The SS316 cladding is filled with helium. Each of the segments is filled with liquid sodium, which works as a heat transfer medium between fuel and heat pipes.

Above and below the reactor core is a SS316 axial reflector. The radial reflector consists of $Al_2O_3$, a helium gap, SS316 shielding to protect from gamma radiation and enriched $B_4C$ to protect it from neutron irradiation.

For reactivity control, 12 rotating control drums situated around the reactor core with semicircular cut-outs of enriched $B_4C$ are used. The rotation of the drums can be used to increase/decrease neutron absorption and thus control the reactivity. Safety rods (inner and annular outer) that are used for safe shutdown are also made up of enriched $B_4C$.

### 2.3. Thermal Expansion

The dimensions given in Table 6 are considered in the shutdown state (at a temperature of 293 K). When the reactor is heated to the operating condition, thermal expansion and a change in density will occur. The linear length expansion has been considered according to:

$$L(T) = L_0 \cdot (1 + \bar{\alpha}\Delta T), \tag{1}$$

where $L(T)$ and $L_0$ are final and initial dimensions, respectively, $\bar{\alpha}$ is an average thermal expansion coefficient, and $\Delta T$ is a temperature difference between the final and initial state.

The following relation was considered for the density changes:

$$\rho(T) = \rho_0 \cdot \frac{1}{(1 + \bar{\alpha}\Delta T)^n}, \tag{2}$$

where $\rho(T)$ and $\rho_0$ are final and initial densities, respectively, and $n$ is a number of expansion directions.

The densities of materials and their thermal expansion coefficients are given in Table 1. For $\bar{\alpha}$, the mean value for the expansion between initial and final temperatures was considered.

There were considered the radial and axial expansion of fuel rods and the radial expansion of cladding, grids, reactor vessel, and radial reflector.

### 2.4. Differences in the Model

According to [1], it was not possible to determine temperature of radial reflector, interface between radial shieldings, diameter of the outer $B_4C$ shielding,

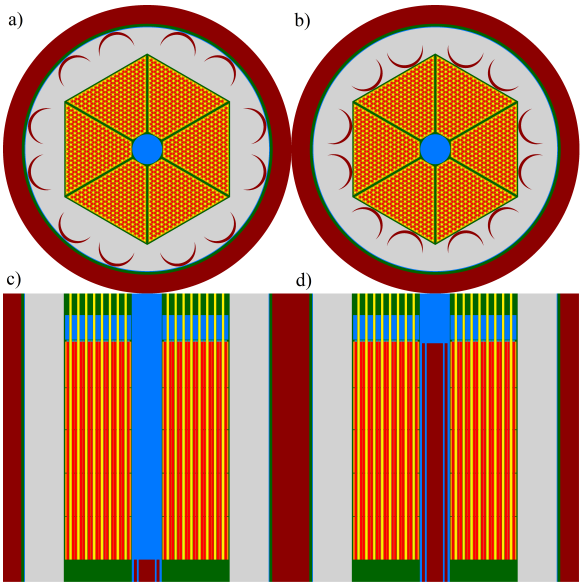


FIGURE 1. Possible positions of the control drums and shutdown rods. a) Control drums in the "out" position, b) control drums in the "in" position, c) shutdown rods in the "out" position, and d) shutdown rods in the "in" position.

and amount of sodium in the vessel. It was therefore necessary to be satisfied with approximate estimates, whose effects on reactivity changes were as follows:

- the estimated radial reflector temperature is 923 K (in the 100 K range, the change in reactivity is roughly **28 pcm**),
- the estimated interface between shieldings is 87 cm in radius (in the 1 cm range, the change is approximately **52 pcm**),
- the estimated size of outer shielding is 100 cm in radius (without change),
- the estimated amount of sodium in the vessel is 152 cm in depth (in the 1 cm range, the change is roughly **12 pcm**).

## 3. RESULTS

### 3.1. REACTIVITY OF THE SYSTEM

Reactivity can be controlled in several ways. The most important is control by control drums rotation, which are changing neutron absorption. Shutdown rods are used for safety shutdown.

In the following text, the "in" position represents the state where all elements have the greatest influence on reactivity. In contrast, the "out" position represents the state with the lowest influence on reactivity, as can be seen in Figure 1.

When all control elements are in the "out" position, a supercritical system is created. The maximum excess reactivity at the Beginning of Life (BOL) is:

$$\varrho_{\max}^{\mathrm{BOL}} = (1543 \pm 2)\ \mathrm{pcm}.$$

To achieve criticality, it is necessary to rotate the control drums by 51° and 318°, respectively, where this rotation is symmetrical for all drums. For a more

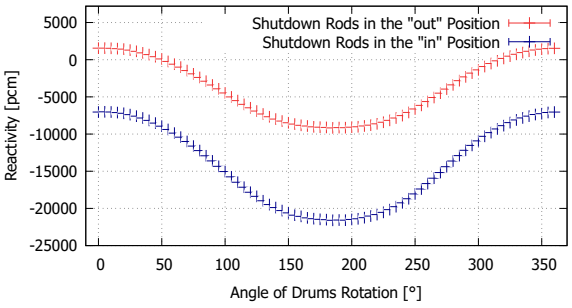


FIGURE 2. Dependency of reactivity on control drums rotation angle.

even power distribution, the 51° position is preferable, therefore all the following calculations were done for this position. The dependency of reactivity on control drums rotation angle is shown in graph in Figure 2.

Table 2 shows the worths of the safety components and compares them with the values from [1] (calculated using MCNP 6.1 code and ENDF/B VII.0 nuclear data library). The calculations in this work showed lower $k_{\mathrm{eff}}$, which is associated with lower BOL excess reactivity. This discrepancy may be due to either a different model or the use of a different nuclear data library. Another aspect is the original study does not describe exact position and shape of axial reflectors, so axial neutron leakage has also a large influence.

When comparing the worths of the safety systems, the results in this work are slightly higher, which is probably due to the same reasons.

From a safety point of view, the control drums are the most important. Important are also the shutdown rods (when inserting at the same time), the outer annular rod and the inner rod. Due to the small

| | **MCNP 6.1** [1] ENDF/B VII.0 | **Serpent 2** ENDF/B VIII.0 |
|---|---|---|
| Critical Drums Rotation [°] | 56 | 51/318 |
| $\beta_{\text{eff}}$ [%] | 0.7 | 0.7199 ± 0.0002 |
| BOL Excess Reactivity [pcm] | 2 359 | 1 543 ± 2 |
| Total Drums Worth [pcm] | 9 079 | 10 677 ± 3 |
| Individual Drum Worth [pcm] | 770 | 866 ± 3 |
| Inner Rod Worth [pcm] | 6 013 | 6 148 ± 3 |
| Annular Rod Worth [pcm] | 7 504 | 7 754 ± 3 |
| Both Rods Worth [pcm] | - | 8 583 ± 3 |

Table 2. Worths of the safety components.

| | **MCNP 6.1** [1] ENDF/B VII.0 | **Serpent 2** ENDF/B VIII.0 |
|---|---|---|
| Fuel Doppler Broadening [pcm/K] | -0.9485 | -0.608 ± 0.010 |
| Fuel Axial Elongation [pcm/K] | -0.3234 | -0.242 ± 0.005 |
| Radial Reflector Expansion [pcm/K] | -0.1575 | -0.142 ± 0.004 |
| Sodium Volume Expansion [pcm/K] | -0.0723 | -0.16 ± 0.03 |
| Grids Expansion [pcm/K] | - | -0.586 ± 0.013 |
| **Total [pcm/K]** | **-1.5017** | **-1.74 ± 0.03** |

Table 3. Temperature reactivity coefficients.

excess reactivity, the individual control elements are able to shutdown the reactor.

### 3.2. Reactivity Coefficients

Reactivity coefficient can be defined according to:

$$a_x = \frac{\partial \varrho}{\partial x}, \tag{3}$$

where $x$ is the parameter (temperature, power, etc.), and $\varrho$ is the reactivity. The numerical determination can be based on the linear fit:

$$f(x) = k \cdot x + b. \tag{4}$$

That means

$$a_x \approx k. \tag{5}$$

Temperature reactivity coefficients are calculated in this paper (i.e. $x$ is $T$).

#### 3.2.1. Doppler Broadening

The fuel Doppler broadening effect has the greatest influence on the change in reactivity with temperature change. The dependency of the $k_{\text{eff}}$ on fuel temperature change shows graph in Figure 3.

The effective multiplication factor and reactivity decrease with increasing temperature. For the operating temperature (at a temperature of 1050 K), the reactivity coefficient of Doppler broadening is:

$$a_T^{\text{Dopp.}} \approx (-0.608 \pm 0.010)\ \text{pcm/K}.$$

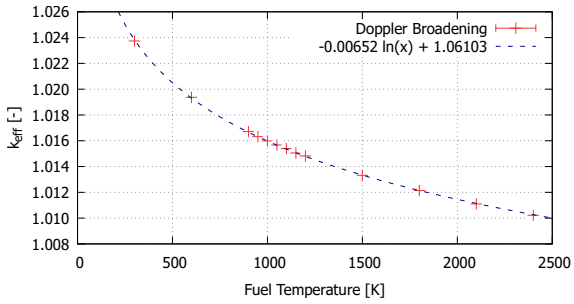


Figure 3. Doppler broadening effect in the fuel.

#### 3.2.2. Thermal Expansion Effects

Other thermal aspects include axial elongation of fuel rods, radial expansion of reflector, volume expansion of sodium, and radial expansion of fuel grids. The densities and the fuel pitch in lattice are changing by thermal expansion, which affects the moderation properties and macroscopic cross-sections. Table 3 shows the calculated temperature reactivity coefficients in these cases. To convert the dimensions and densities, the Relations (1) and (2) were used, so that the total mass of all components remained constant.

All the temperature reactivity coefficients are negative, which is important for the safe operation of the reactor. Most of all obtained values are smaller in absolute value compared to those in [1]. In addition, the influence of the expansion of fuel grids and thus the changing fuel pitch was also calculated. This aspect was not considered in [1], however, its value is not negligible and it is the second largest reactivity coefficient after the fuel Doppler broadening.

| | **MCNP** [1] ENDF/B VII.0 | **conf. 51°** ENDF/B VIII.0 | **conf. 318°** ENDF/B VIII.0 |
|---|---|---|---|
| Total Heat Power [MW] | 5 | 5 | 5 |
| Number of Fuel Pins [-] | 2 112 | 2 112 | 2 112 |
| Average Pin Power [kW] | 2.37 | 2.37 | 2.37 |
| Maximum Pin Power [kW] | 2.84 | 2.903 ± 0.002 | 2.916 ± 0.002 |
| Minimum Pin Powe!r [kW] | - | 1.983 ± 0.002 | 1.598 ± 0.002 |
| Radial Peaking Factor [-] | 1.20 | 1.22 | 1.23 |
| Axial Peaking Factor [-] | 1.27 | 1.30 | 1.30 |
| Average Power Density [W/cm$^3$] | 9.03 | 9.03 | 9.03 |
| Maximum Pin Power Density [W/cm$^3$] | 10.82 | 10.82 ± 0.01 | 10.87 ± 0.01 |
| Maximum Power Density [W/cm$^3$] | - | 14.05 ± 0.04 | 14.15 ± 0.04 |

TABLE 4. Thermal power parameters.

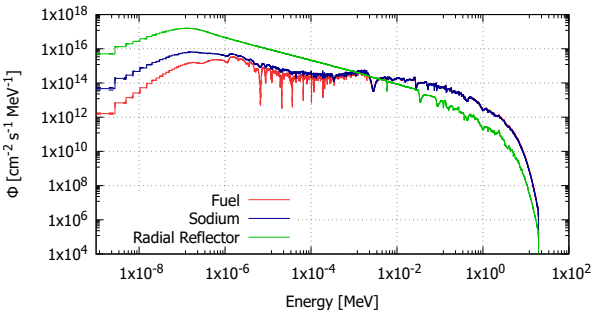


FIGURE 4. Neutron spectra.

### 3.3. Neutron Spectra

Next, the average neutron spectra in fuel, sodium, and in radial reflector were calculated using the ECCO-1968 group structure.

As can be seen in Figure 4, the spectrum in reflector corresponds to the thermal spectrum. For fuel and sodium, there is a shift of neutron energies to higher values. The reactor neutron energy spectrum is shaped by the uranium enrichment, the size of the core, and the large reflector layer and as a result, it is neither a spectrum of a fast reactor nor spectrum of a thermal reactor.

### 3.4. Power Distribution

As it was already mentioned, the pin power distribution very much depends on the choice of the critical state. As can be seen in Figure 5, if a more even power distribution is desired, it is preferable to select a critical state at 51° control drums rotation. In the 318° critical configuration, some of the fuel rods around the perimeter would burn significantly less compared to the 51° configuration, which results in a greater temperature gradient.

The results here show that the control drums not only affect the overall reactivity in the system but also affect the radial distribution of the neutron flux, because they significantly affect the neutron absorption in the system.

Table 4 shows the calculated power outputs in the fuel pins (average, maximum, and minimum). Max-

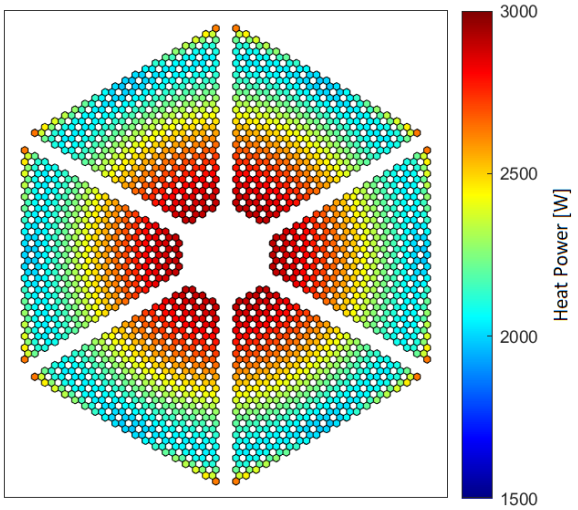


(A).

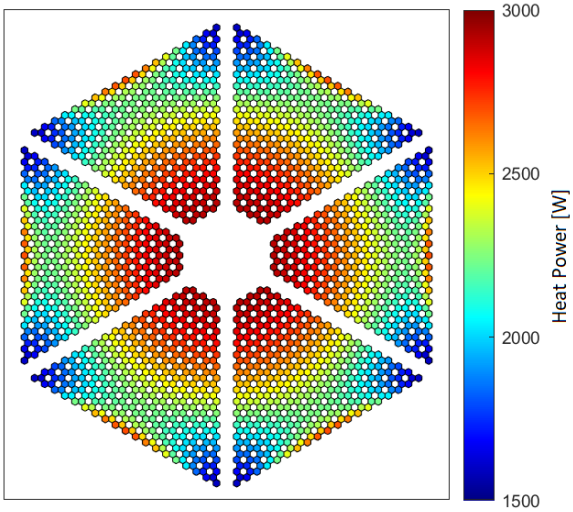


(B).

FIGURE 5. Power distribution in the 51° configuration (a) and in the 318° configuration (b).

| | BOL | EOL |
|---|---|---|
| $\beta_{\text{eff}}$ [%] | 0.7199 ± 0.0002 | 0.7180 ± 0.0009 |
| Excess Reactivity [pcm] | 1 543 ± 2 | 1 297 ± 9 |
| Total Drums Worth [pcm] | 10 677 ± 3 | 10 773 ± 14 |
| Individual Drum Worth [pcm] | 866 ± 3 | 904 ± 12 |
| Inner Rod Worth [pcm] | 6 148 ± 3 | 6 206 ± 13 |
| Annular Rod Worth [pcm] | 7 754 ± 3 | 7 829 ± 13 |
| Both Rods Worth [pcm] | 8 583 ± 3 | 8 647 ± 13 |

Table 5. Worths of the safety components at BOL and at EOL.

imum power output in one fuel rod in both critical configurations is very similar and does not exceed 3 kW. The same is for the radial peaking factor, which is 1.22 and 1.23 for the 51° and 318° configurations, respectively. However, the minimum power generated in the pins differs significantly, which is approximately 400 W less for the 318° configuration.

### 3.5. Burnup

The predictor-corrector method implemented in Serpent 2 code was used for the depletion calculation. For the calculation, the fuel was divided into 63 360 zones. This division occurred at the level of individual fuel rods and was further subdivided into 30 axial sub-zones. The depletion took place in parallel on 32 threads with an allocated memory of 62.5 GB. Standard isotopes, and `set opti 2` memory optimization were considered.

The final burnup of the core allows long depletion steps, but still, shorter steps were defined for the beginning of the depletion calculation to respect faster initial changes in concentrations of short-lived radionuclides. The final depletion steps were 1, 2, 5, 10, 20, and 50 days, and then in half-year steps up to 5 years.

#### 3.5.1. Change in Reactivity

The multiplication factor decreases roughly linearly during the depletion (see Figure 6). Due to the small burnup (1.77 MWd/kgU over 5 years at nominal power), the reactor is still supercritical at the End of Life (EOL):

$$\varrho_{\text{max}}^{\text{EOL}} = (1297 \pm 9) \text{ pcm}.$$

The effective fraction of delayed neutrons (see Table 5) differs in this case mainly because of the statistics. Physically, it should be different mainly due to conversion of $^{238}$U to fissile isotope $^{239}$Pu with much lower fraction of delayed neutrons compared to $^{235}$U.

The effect of burnup can also change the worths of control elements, because it shifts the power distribution to the periphery, leading to greater neutron leakage. Since the reactor is regulated by control drums, their efficiency should change.

There was an increase in all worths during the calculation (see Table 5), but due to the larger statistical uncertainties, the worths of the elements are roughly

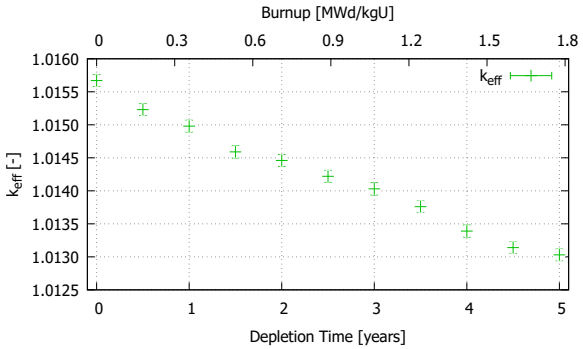


Figure 6. Change in multiplication factor over 5 years.

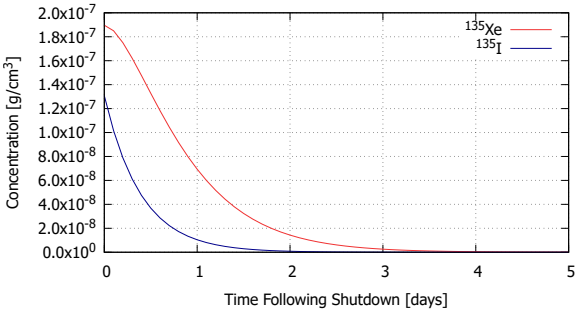


Figure 7. Dependency of $^{135}$I and $^{135}$Xe concentration on time after shutdown.

constant over time. Thus, during operation, it would be possible to maintain criticality using only a slight rotation of the control drums.

#### 3.5.2. Iodine and Xenon

For the reactor operation in remote locations, the power output would need to be changed over time as needed. If xenon poisoning were to occur in the system, this would be very difficult, if not impossible, to regulate. The concentrations of isotopes $^{135}$I and $^{135}$Xe were calculated over 5 days after shutdown. Due to the low power, accumulation of the $^{135}$I isotope is not sufficient to produce a $^{135}$Xe concentration peak, as can be seen in Figure 7. Thus, xenon dead time does not occur.

#### 3.5.3. Power Distribution

As was mentioned above, the effect of burnup should shift the power distribution to the periphery. In this

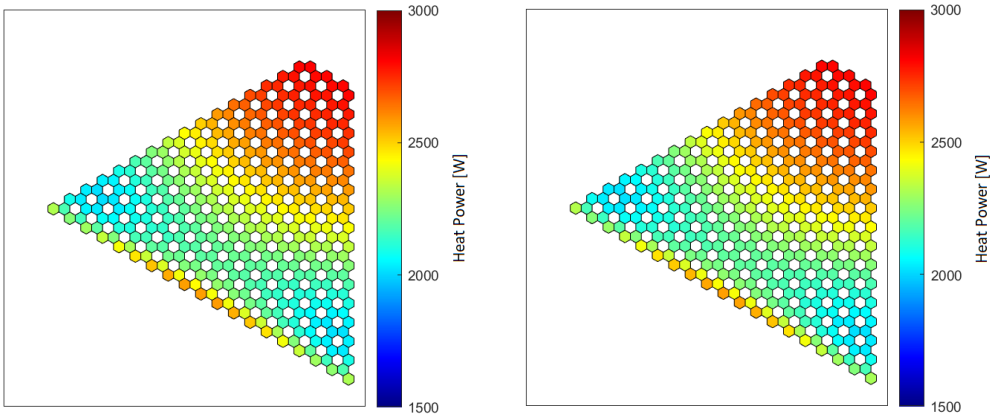


(A). (B).

FIGURE 8. Power distribution at BOL (left) and EOL (right) in the 0° configuration.

analysis, the neutron flux was not sufficient and even in 5 years there was no significant shift. A maximum difference was achieved up to 1 % between BOL and EOL, but this difference may be due to statistical uncertainties. The power distribution is roughly constant over time, as can be seen in Figure 8.

### 3.6. Decay Heat

It was found that at the moment of shutdown, the decay heat power reaches 329.1 kW, which is about 6.58 % of the nominal power. Further, there is a decrease following the decay of accumulated radionuclides, as can be seen in Figure 9.

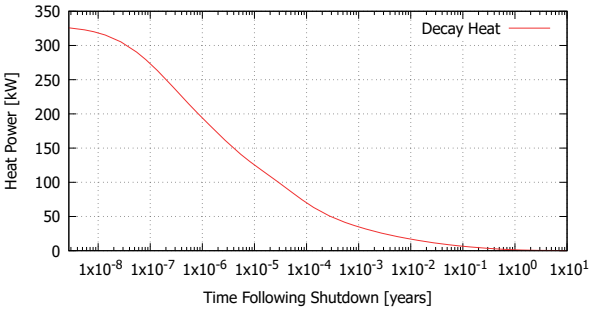


FIGURE 9. Decay heat after shutdown.

## 4. Conclusions

In this paper, the neutronic model of the SPR Design-B nuclear reactor concept from INL is described and basic safety analyses are calculated. All calculations were performed using Monte Carlo code Serpent 2 and nuclear data library ENDF/B VIII.0. The calculation model respects the material temperature field from the reference calculation [1], so thermal-mechanical feedbacks are not included.

The first section provided a necessary context for understanding this topic. Advantages of HPC reactors for their specific applications, such as scientific and military stations, and space applications were summarized. Furthermore, the development of HPC reactors in LANL and INL has been described.

The second section deals with the calculation model itself. Thermal expansions, dimensional changes and density changes were considered. All the materials, their composition, expansion coefficients, and densities were taken from available references. A basic sensitivity analysis was made to assess the impact estimations of compositions and dimensions not available in the reference calculation.

In the third section, the results are discussed and also compared with the original INL study [1], where MCNP 6.1 code with ENDF/B-VII.0 nuclear data library was used for the calculations.

All the values obtained are very similar. All feedback coefficients are negative, as well as the worths of safety elements are high enough to shutdown the reactor. The worths increase during depletion, but due to the larger statistical uncertainties, they are roughly constant over time.

The biggest differences are in the lower multiplication factor in this work. This may be due to a different model, a different nuclear data library with different code, or due to an axial neutron leakage. Since the exact position and shape of axial reflectors at INL were not provided, a comparison of the axial power distribution between INL and this study was conducted. Differences were identified, with the most significant disparities occurring at the bottom of the reactor core. These discrepancies suggest that variations in the multiplication factor were likely primarily caused by axial leakage.

It was found a critical position of control drums at an angle of 51°, where the most even power distribution is obtained. In burnup calculation (5 years at a nominal heat power output of 5 MW), it was found that the $^{135}$I concentration is not sufficient to cause a xenon dead time. When the reactor is shutdown after 5 years, the decay heat reaches 6.56 % of the nominal power.

## List of symbols

$a_T$ Temperature Reactivity Coefficient [pcm/K]
$\alpha$ Thermal Expansion Coefficient [1/K]
$B$ Burnup [MWd/kgU]
$\beta_{\text{eff}}$ Effective Fraction of Delayed Neutrons [%]
$E$ Energy [MeV]
$k_{\text{eff}}$ Effective Multiplication Factor [–]
$L$ Length [cm]
$m$ Mass [kg, g]
$n$ Number of Expansion Directions [–]
$\phi$ Normalized Neutron Flux [1/s/cm$^2$/MeV]
$P$ Thermal Power [MW, kW]
$p$ Thermal Power Density [W/cm$^3$]
$\rho$ Density [g/cm$^3$]
$\varrho$ Reactivity [pcm]
$T$ Temperature [K]

## List of Abbreviations

BOL Beginning of Life
EOL End of Life
HPC reactor Heat-pipe Cooled reactor
INL Idaho National Laboratory
LANL Los Alamos National Laboratory
SPR Special Purpose Reactor
SS316 316 Stainless Steel

## Acknowledgements

This analysis was partially supported by ESA project Preliminary European Reckon on Nuclear Electric Propulsion for Space Applications (RocketRoll), ESA ITT/1-11474/22/FR/KR.

## References

[1] J. W. Sterbentz, J. E. Werner, A. J. Hummel, et al. Preliminary Assessment of Two Alternative Core Design Concepts for the Special Purpose Reactor. Tech. rep., Idaho National Lab. (INL), Idaho Falls, ID (United States), 2017. https://doi.org/10.2172/1413987

[2] Nuclear Reactors and Radioisotopes for Space, 2021. [2022-10-06]. https://world-nuclear.org/information-library/non-power-nuclear-applications/transport/nuclear-reactors-for-space.aspx

[3] D. I. Poston, R. J. Kapernick, R. M. Guffee. Design and analysis of the SAFE-400 space fission reactor. *AIP Conference Proceedings* **608**(1):578–588, 2002. https://doi.org/10.1063/1.1449775

[4] D. I. Poston, R. J. Kapernick, R. M. Guffee, et al. Design of a heatpipe-cooled Mars-surface fission reactor. *AIP Conference Proceedings* **608**(1):1096–1106, 2002. https://doi.org/10.1063/1.1449841

[5] R. S. Reid, J. T. Sena, A. L. Martinez. Sodium heat pipe module test for the SAFE-30 reactor prototype. *AIP Conference Proceedings* **552**(1):869–874, 2001. https://doi.org/10.1063/1.1358021

[6] D. I. Poston, M. A. Gibson, R. G. Sanchez, P. R. McClure. Results of the KRUSTY nuclear system test. *Nuclear Technology* **206**(sup1):S89–S117, 2020. https://doi.org/10.1080/00295450.2020.1730673

[7] P. R. Mcclure, D. I. Poston, V. R. Dasari, R. S. Reid. Design of megawatt power level heat pipe reactors. Tech. rep., Los Alamos National Lab. (LANL), Los Alamos, NM (United States), 2015. https://doi.org/10.2172/1226133

[8] J. W. Sterbentz, J. E. Werner, M. G. McKellar, et al. Special Purpose Nuclear Reactor (5 MW) for Reliable Power at Remote Sites Assessment Report. Tech. rep., Idaho National Lab. (INL), Idaho Falls, ID (United States), 2017. https://doi.org/10.2172/1410224

[9] J. Leppänen, M. Pusa, T. Viitanen, et al. The Serpent Monte Carlo code. In *Annals of Nuclear Energy*, vol. 82, pp. 142–150. 2015. https://doi.org/10.1016/j.anucene.2014.08.024

[10] D. A. Brown, M. B. Chadwick, R. Capote, et al. ENDF/B-VIII.0: The 8$^{\text{th}}$ major release of the nuclear reaction data library with CIELO-project cross sections, new standards and thermal scattering data. In *Nuclear Data Sheets*, vol. 148, pp. 1–142. 2018. Special Issue on Nuclear Reaction Data. https://doi.org/10.1016/j.nds.2018.02.001

[11] Potassium – thermophysical properties vs. temperature, 2008. [2023-01-21]. https://www.engineeringtoolbox.com/potassium-properties-d_1210.html

[12] J. K. Fink, L. Leibowitz. Thermodynamic and transport properties of sodium liquid and vapor. p. 87. Argonne National laboratory, 1995. https://doi.org/10.2172/94649

[13] V. D. Arp, R. D. McCarty, D. G. Friend. Thermophysical properties of helium-4 from 0.8 to 1500 K with pressures to 2000 MPa. In *NIST Technical Note 1334 (revised)*. NIST, 1994.

[14] R. J. McConn, C. J. Gesh, R. T. Pagh, et al. Compendium of material composition data for radiation transport modeling. In *Homeland Security*, pp. 285–290. 2011. https://doi.org/10.2172/1023125

[15] J. S. Coursey, D. J. Schwab, J. J. Tsai, et al. NIST Physical Measurement Laboratory, Atomic Weights and Isotopic Compositions with Relative Atomic Masses, 2021. [2023-01-20]. https://physics.nist.gov/cgi-bin/Compositions/stand_alone.pl?ele=&all=all&ascii=ascii&isotype=all

[16] *Thermophysical Properties Database of Materials for Light Water Reactors and Heavy Water Reactors*. No. 1496 in TECDOC Series. IAEA, 2006.

[17] Coefficients for austenitic stainless steels (group 3). In *BPVC Section II Part D (Metric)*, p. 806. ASME, 2017.

[18] International Syalons, Alumina, Aloxalon 999 - Physical Property Data, 2023. [2023-01-20]. https://www.syalons.com/materials/alumina/

# A. Appendix

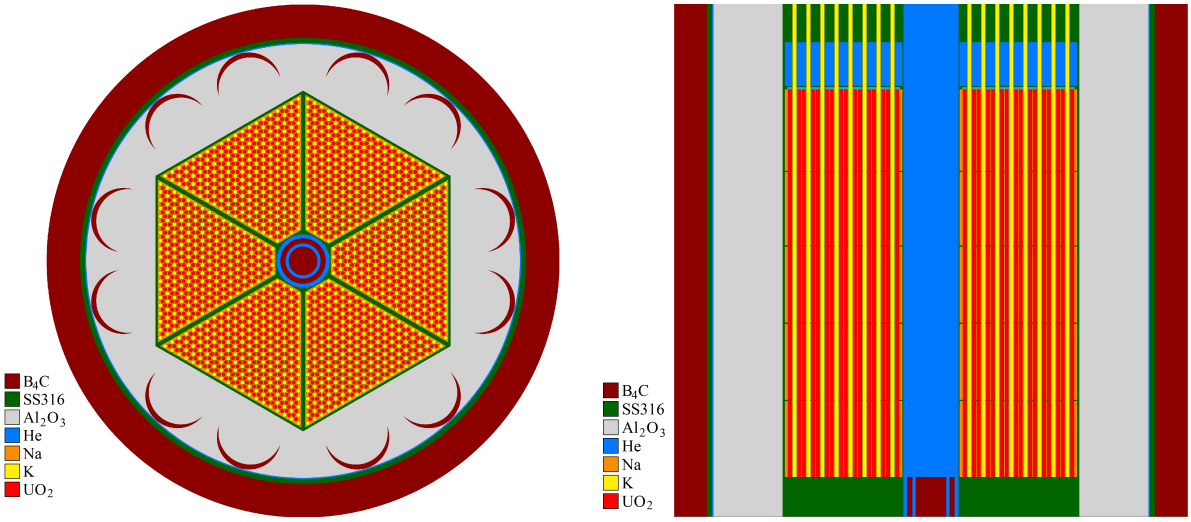


(A). (B).

FIGURE 10. Horizontal (left) and vertical (right) cross section of the model.

| **Fuel Rod** | |
|---|---|
| Number | 2,112 |
| Material | $UO_2$ |
| Enrichment | 19.75 % |
| Diameter | 1.492 cm |
| Length | 150 cm |
| Pitch | 1.8 cm |
| Temperature | 1050 K |
| **Cladding** | |
| Material | SS316 |
| Gap | He |
| Diameter | 1.505–1.565 cm |
| Temperature | 1013 K |
| **Heat Pipe** | |
| Number | 1,224 |
| Material | SS316 |
| Filling | K (100 g) |
| Diameter | 1.575–1.775 cm |
| Temperature | 986 K |
| **Heat Transfer Medium** | |
| Material | liquid Na |
| Temperature | 995 K |

| **Axial Reflector** | |
|---|---|
| Material | SS316 |
| Height | 15 cm |
| **Radial Reflector** | |
| Material | $Al_2O_3$ |
| Outer Diameter | 168.1 cm |
| Height | 200 cm |
| Temperature | 923 K |
| **Control Drums** | |
| Amount | 12 |
| Diameter | 25 cm |
| Absorbtion Material | $B_4C$ (90 % $^{10}B$) |
| Maximum Thickness | 2 cm |
| **Shutdown Rods** | |
| Material | $B_4C$ (90 % $^{10}B$) |
| Diameter of Inner Rod | 11.2 cm |
| Diameter of Annular Rod | 13.7–17.7 cm |
| **Shielding** | |
| SS316 Shielding Diameter | 170.1–174 cm |
| $B_4C$ Shielding Diameter | 174–200 cm |

TABLE 6. Parameters of the SPR Design-B nuclear reactor concept [1].